

Lagrangian tracer homogenization and dispersion in a simplified atmospheric GCM (*)

M. BAGLIANI⁽²⁾(¹), K. FRAEDRICH⁽¹⁾, J. VON HARDENBERG⁽²⁾(¹)(**) and F. LUNKEIT⁽¹⁾

⁽¹⁾ *Meteorologisches Institut, Universität Hamburg - Hamburg, Germany*

⁽²⁾ *Istituto di Cosmogeofisica, CNR - C.so Fiume 4, I-10133 Torino, Italy*

(ricevuto il 18 Novembre 1999; approvato il 21 Febbraio 2000)

Summary. — Lagrangian transport in the atmosphere is numerically studied by using a simplified general circulation model (SGCM) with Newtonian cooling and Rayleigh friction. Long-term Lagrangian behaviour is analyzed by determining hemispheric and global homogenization times and by studying the time evolution of tracer distributions. At short times, the properties of absolute dispersion are considered. The tracer dynamics reveals the presence of transport barriers associated with slow inter-hemispheric and troposphere-stratosphere exchanges, and with a slow crossing of the boundary between the Ferrel and Hadley cells.

PACS 92.60.Bh – General circulation.

PACS 92.60.Mt – Particles and aerosols.

PACS 92.60.Ry – Climatology.

1. – Introduction

Transport of Lagrangian tracers plays an important role in atmospheric dynamics. In past years, different approaches to the study of this problem have been pursued. One of them is based on the use of high-resolution, sophisticated general circulation models (GCMs) of the atmosphere. This approach can be useful for reproducing realistic Eulerian conditions, it has the disadvantage, however, that the numerical complexity of most GCMs makes it very costly to run the models for long times and/or to conduct sensitivity studies. Consequently, in this framework it is often difficult to identify the main elementary physical processes at work and to disentangle their respective roles.

A different approach is based on the use of simplified kinematic flow models, employing the notion of chaotic advection and concepts from dynamical system theory. In this way, it is possible to separate the properties of Lagrangian advection from those of the Eulerian dynamics (which is given as a prescribed kinematic flow) and study the

(*) The authors of this paper have agreed to not receive the proofs for correction.

(**) E-mail: jost@icg.to.infn.it

role of individual entities such as large-scale Rossby waves and isolated vortex structures [1-4]. This approach has provided several interesting results, but it has the disadvantage that it is often too simplified to model the complex interactions in the real atmosphere.

A possible answer to the dichotomic desire of keeping the Eulerian dynamics simple but at the same time not completely unrealistic is provided by the family of the so-called simplified general circulation models (SGCMs), which provide a numerical solution to the primitive equations on the sphere, with simplified (linear) parameterization of the unresolved processes and with intermediate spatial resolution. These models, although obviously much less realistic than a full GCM, do indeed contain many of the relevant atmospheric processes and can be integrated for long times, considering many different initial conditions and parameter values. Following this approach, here we report on a study of Lagrangian transport in the dry SGCM called PUMA (Portable University Model of the Atmosphere), considering meridional transport and dispersion.

2. – Characteristics of the model

2.1. Physical and numerical background. – The PUMA model has been developed at the University of Hamburg by modifying the early Reading spectral model described in refs. [5, 6]. Further details are given in refs. [7-9].

PUMA integrates the primitive equations for a dry atmosphere on a spherical domain. Dynamical variables are vorticity, divergence, temperature and the logarithm of surface pressure. In the runs discussed here, no orography is present. The model employs σ coordinates along the vertical, $\sigma = p/p_s$, where p is the pressure and p_s is the pressure at the surface of the sphere.

The PUMA model uses simplified, linear parameterizations of the physical processes that are not explicitly resolved. The vertical is discretized by equally spaced σ -levels. Diffusion and subgrid turbulent mixing are parameterized by a hyperdiffusion term: $(-1)^{q-1} K_q \nabla^{2q} S$, where S is the generic field variable and K_q is the hyperdiffusion coefficient. In the following, we use $q = 3$.

Turbulent momentum exchange and surface drag are represented by a Rayleigh friction term $-S/\tau_D$, added to the vorticity and divergence equations. Here τ_D is the timescale of subgrid momentum mixing and it is a function of the vertical coordinate. Diabatic processes such as radiative and convective heating are described by a Newtonian cooling term $(T_E - T)/\tau_E$ in the temperature equation. This term forces the model temperature T to relax toward the temperature profile T_E with characteristic timescale τ_E . The temperature profile $T_E(\phi, \sigma, t)$ represents the equilibrium profile induced by solar heating. No parameterizations for additional vertical mixing or convective adjustment are included.

The model equations, in non-dimensional form, are numerically solved using a pseudo-spectral method [10, 11], linear terms are evaluated in spectral space and nonlinear products are calculated in physical space. The model uses a spectral representation in the horizontal and a finite difference scheme in the vertical. The time integration is performed by a leap-frog semi-implicit scheme [12]. The simulations discussed in this work are based on the triangular truncation T42 corresponding to a Gaussian grid of approximately $2.8^\circ \times 2.8^\circ$, with 10 vertical σ -levels. The timescale of Newtonian cooling is set to $\tau_E = 30$ days for all the vertical layers. The timescale of

momentum transfer is set to $\tau_D = 1, 5, 10$ days for the lower three levels (where $\sigma = 0.95, 0.85, 0.75$, respectively) and to $\tau_D = \infty$ elsewhere.

2.2. Solar forcing: perpetual and seasonal cycle. – The PUMA runs discussed in this work employ either a time-independent mean solar input or a solar forcing with seasonal cycle. In the case of constant solar input (perpetual runs), the temperature field T_E is kept constant in time during the whole integration. In this case, we set $\Delta T_{NS} = 30$ K and $\Delta T_{EP} = 60$ K, where ΔT_{NS} and ΔT_{EP} represent, respectively, the North Pole-South Pole and North Pole-Equator temperature difference. In this way PUMA simulates a climate situation with perpetual summer in the northern hemisphere. For the seasonal runs, the value of ΔT_{NS} is allowed to vary sinusoidally in time with a period of 360 days. Consistency between seasonal and perpetual runs is achieved by requiring the same mean annual solar energy input in the two cases.

Using the two types of forcing, we have computed the time and zonal means of potential temperature, horizontal velocity and meridional mass stream function. Averages have been taken over a period of 10 years. Seasonal and perpetual runs have similar Eulerian averages and in the following we discuss the average Eulerian properties of the perpetual runs only.

In general, the mean properties of the observed zonally averaged atmospheric circulation are reasonably captured in the simulations. However, some deficiencies are natural, taking into account the substantial simplifications regarding the representation of the physical processes and, in particular, the lag of moisture. The model climatology is illustrated by the potential temperature and zonal mean wind profiles (fig. 1a)) and the meridional mass stream function (fig. 1b)). The potential temperature profile is in good agreement with observations in the troposphere, while the stratosphere is poorly represented due to the limited number of vertical levels in the model. The zonal mean wind displays mid-latitude jets whose strength is comparable to observations in the atmosphere [13]. Also the tropical easterlies are well described. The jets, mainly in the winter season (southern hemisphere), show a shape characterized by two maxima, corresponding to the subtropical and mid-latitude jets observed in the southern hemisphere. The model is able to reproduce the circulation in the Hadley, Ferrel and polar cells, although the numerical values of the meridional mass stream function are weaker than the measured ones. In particular, the strength of the Hadley cell is significantly underestimated, while the maximum is located much too low. Both features can be attributed to the lack of moist processes in PUMA.

2.3. Tracer advection. – The motion of a passively advected particle is described by the equations

$$(1) \quad \frac{d\mathbf{r}}{dt} = \mathbf{v}(\mathbf{r}, t),$$

where \mathbf{r} is the particle position at time t and $\mathbf{v}(\mathbf{r}, t)$ is the Eulerian velocity at position \mathbf{r} and time t . The velocity has “horizontal” components u, v defined on the plane tangential to the σ level passing through \mathbf{r} and a “vertical” component w perpendicular to the local σ isosurface. On a sphere, the horizontal components become $\frac{d\lambda}{dt} = \frac{u(\lambda, \phi, t)}{a \cos \phi}$ and $\frac{d\phi}{dt} = \frac{v(\lambda, \phi, t)}{a}$, where a is the Earth radius and λ, ϕ are zonal and meridional coordinates, respectively. Equation (1) is integrated in time by using the

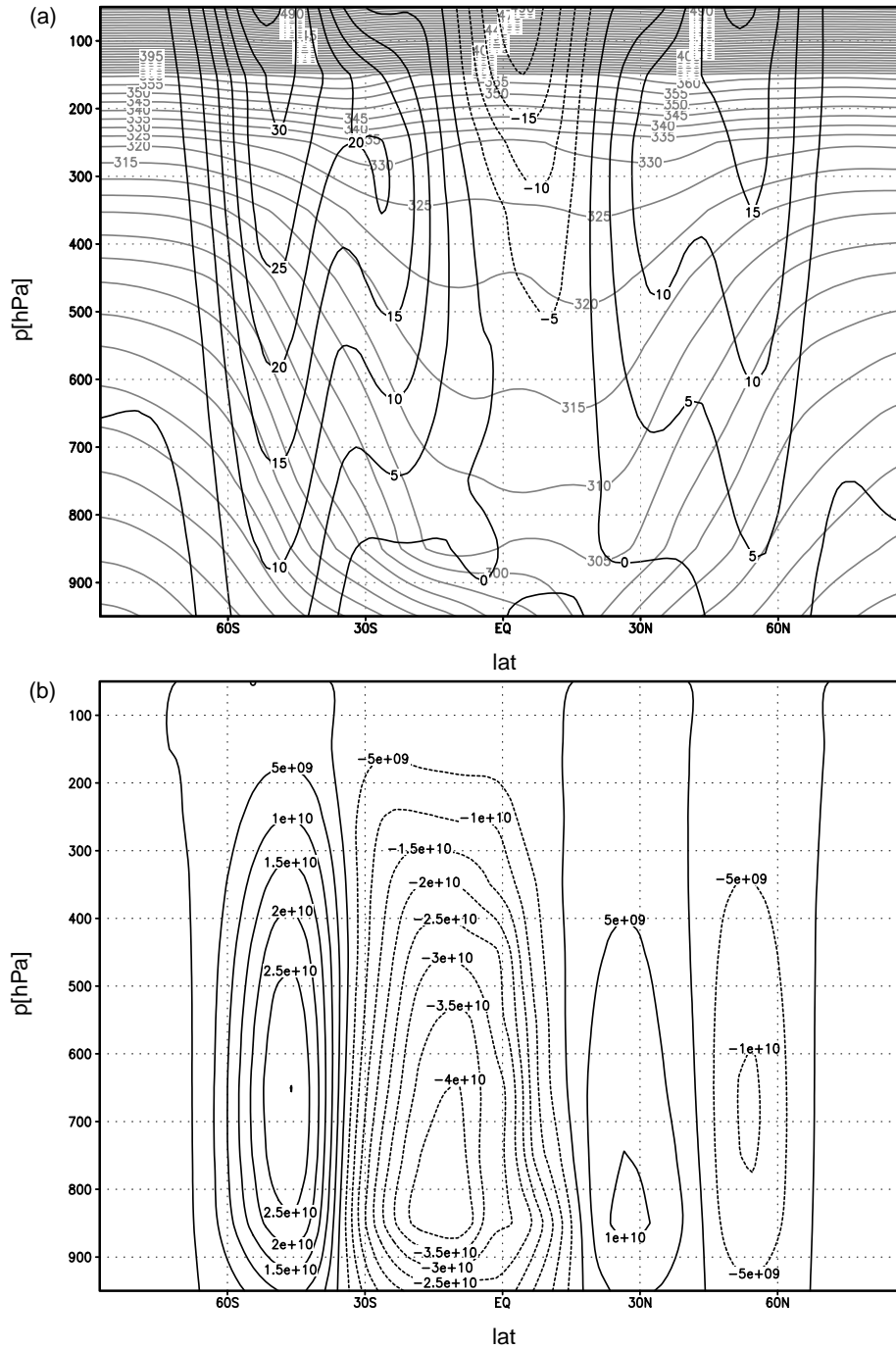


Fig. 1. – (a) Potential temperature (grey, in K) and zonal mean wind (black, in ms^{-1}) profiles. (b) Meridional mass stream function, in 10^{10} kgs^{-1} .

same second-order semi-implicit leap-frog scheme used to integrate the Eulerian model.

Since all the values calculated by the Eulerian model are given on a fixed Gaussian grid, an interpolation scheme is necessary to obtain estimates of the wind velocity at the tracer positions. Two interpolation schemes have been implemented: bicubic splines and bilinear. The advantage of splines over linear interpolation is the continuity of the acceleration on the grid, but this is offset by a significant increase in the required computational time. For this reason, in the following we use the simpler linear interpolation scheme. Test runs comparing the two interpolation schemes have indicated that for the present situation the two procedures provide similar results. The horizontal and vertical ($\dot{\sigma}$) wind velocities are first interpolated on the horizontal, on every model level. Then another interpolation in the vertical provides the wind at the position of each tracer. Horizontal and vertical velocities are assumed to vanish at the upper and lower boundaries $\sigma = 0$ and $\sigma = 1$.

3. – Transport barriers and particle spread

Lagrangian tracers do not spread at an even rate over the entire spherical domain. In particular, there are specific dynamical regions that act as transport barriers. To qualitatively identify transport barriers in the PUMA model, we have performed a 6-month integration of the case with constant solar forcing. In this run, 8192 passive particles are seeded in the whole computational domain, their initial positions coinciding with the model grid points. The passive tracers are released on the isentropic surface at 315 K. This specific isentrope is chosen because it lies mostly within the troposphere and it does not intersect the ground. We can thus avoid the difficult question of tracer sources and sinks within the atmospheric boundary layer. Note, however, that the particle motion is obtained by three-dimensional integration, and the particles are not constrained to stay on the initial isentropic surface. This is at variance with what has been done in early studies of chaotic advection on isentropic surfaces [14] and it is required by the observation that particle motion is generally not adiabatic in the troposphere.

Figure 2a) shows the tracer latitude after 6 months of advection, as a function of their initial latitude. Panel b) reports the initial and final vertical position *vs.* the initial latitude. Figure 2a) suggests the existence of three main transport barriers, located approximately at 60° N, 50° S and 10° N. The latter corresponds to the dynamical Equator, and the first two correspond to the intersections of the 315 K isentrope with the tropopause. North of 60° N and south of 50° S, the selected isentrope lies, respectively, in the winter and the summer stratosphere. Note that these regions have been identified as stratosphere because the potential vorticity gradient on the isentropic surface at 315 K reaches local maxima at about 60° N and 55° S. Furthermore, these latitudes correspond to the positions where the absolute value of potential vorticity on the isentropic surface 315 K is 1.5 PVU. Between 60° N and 50° S, the 315 K isentrope lies in the troposphere. Thus, these barriers should be interpreted in terms of the limited permeability of the tropopause to particle exchanges between the stratosphere and the troposphere, associated with a large value of the potential vorticity gradient in these regions.

Vertical spread, shown in fig. 2b), can be interpreted in a similar way. In the stratosphere, particles tend to remain on the original isentrope, with a few exceptions

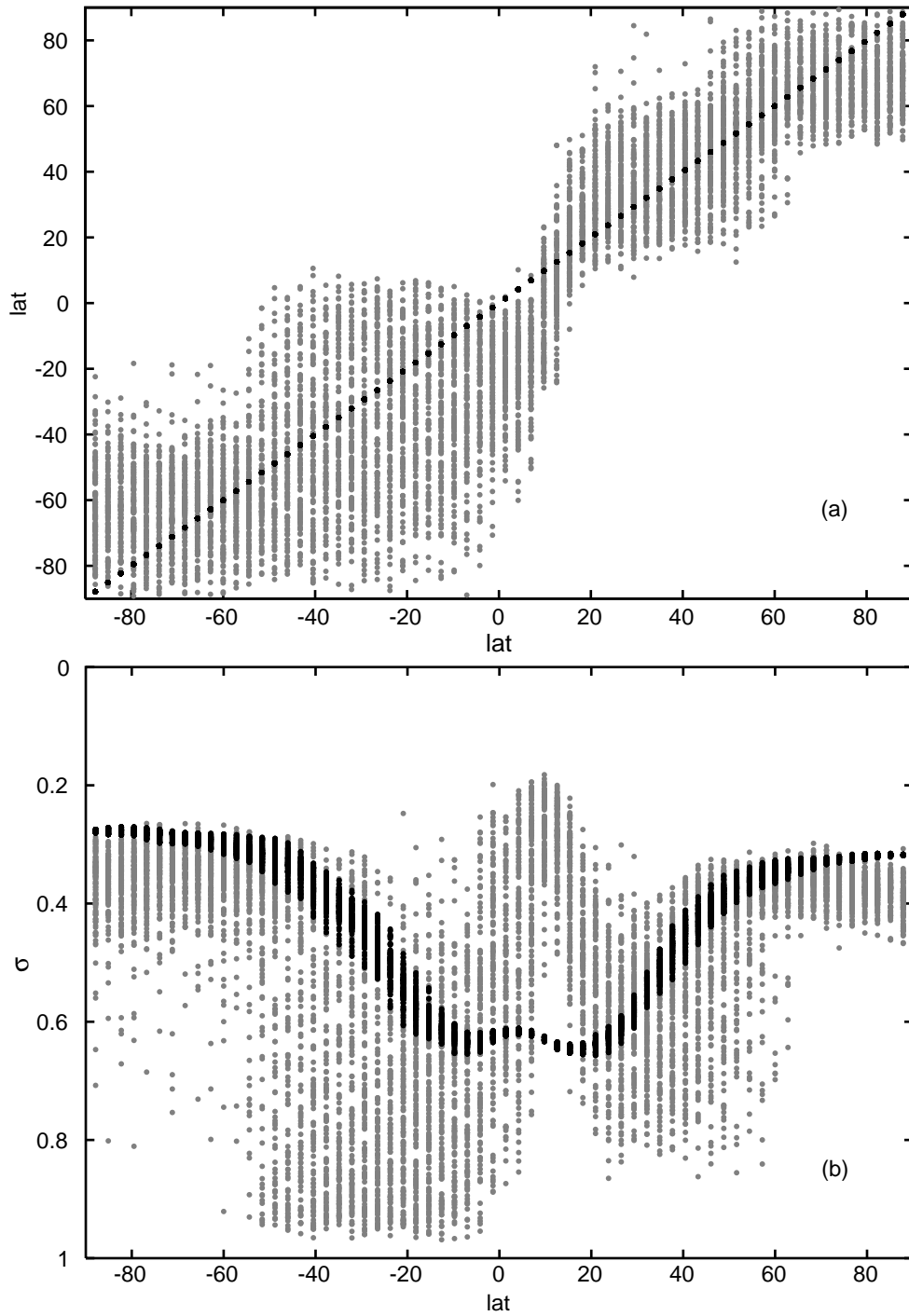


Fig. 2. – (a) Tracer latitude after 6 months of advection, as a function of the initial latitude. (b) Initial and final vertical position of the tracers *vs.* the initial latitude.

in the southern (winter) stratosphere. Between about 60°N and 50°S , the particles participate in the overall circulation, with ascending movements at the Equator and descending motion in subtropical regions.

4. – Long-term behaviour and homogenization times

An important practical question concerns the time that a flow takes to homogenize the distribution of an ensemble of passively advected tracers. This problem has been addressed recently using a 2D zonally averaged model of atmospheric circulation [15].

To study this issue in the PUMA model, we integrated the motion of 30000 passive tracers that were initially released at a fixed latitude, on the isobaric surface at 500 hPa. This pressure surface lies entirely in the troposphere. The tracer motion has been integrated for a total time of 50 years; we used both perpetual solar forcing and a solar input varying with the seasonal cycle.

For the perpetual forcing, we have selected six seeding latitudes at 75°S , 45°S , 15°S , 25°N , 55°N , 80°N , roughly corresponding to the centers of the Hadley, Ferrel and polar cells. Selection of both hemispheres allows for sampling both summer and winter initial conditions. For the run with seasonal forcing, we have selected three seeding latitudes on one hemisphere, at 75°S , 45°S , 15°S . With seasonal forcing, winter and summer alternate in each hemisphere and the dependence on the initial condition disappears after a few years.

Figures 3a), b) show the zonally and vertically averaged probability density function of the particle latitudes for the perennial and seasonal runs, respectively. The PDFs have been normalized by dividing the counting in each bin by the total number of particles and by the width of the bin. The different panels in each figure refer to different instants of time after particle release. For the perennial run, only particles seeded in the southern hemisphere are shown. The dotted line represents the particle distribution with constant density on the whole sphere (globally homogeneous distribution). This latter is given by a cosine function for the latitudinal distribution and by a constant for the distribution along σ levels.

In the first six months of integration, the particle distributions for the perpetual and seasonally forced runs remain similar to each other. Since the seeding sites for this run are located in the troposphere (at variance with the case considered in sect. 3, where seeding was on the 315 K isentrope), the particles do not feel the tropopause barrier. Most of the particles released near the Pole (curves labeled by A) have reached the Equator after six months, sliding downward and equatorward along the slanted isentropes and entering the tropics through the convergence zone near the surface visible in fig. 1.

Once in equatorial regions, these particles tend to rise to upper levels without significant meridional displacement, generating the large particle concentration at the Equator visible in the first panels of figs. 3a), b). Some of the particles released close to the Pole, however, remain at high latitudes, recirculating south of 40°S . A similar behaviour is observed for the particles seeded at 45°S . In general, these particles spend little time in regions between about 30° and 40°S , producing the low particle densities seen at these latitudes.

The behaviour of the particles released at polar (75°S) or temperate (45°S) latitudes can be understood by noting that these particles circulate mainly in the Ferrel cell. Once reached lower latitudes, some particles cross the boundary between the Ferrel

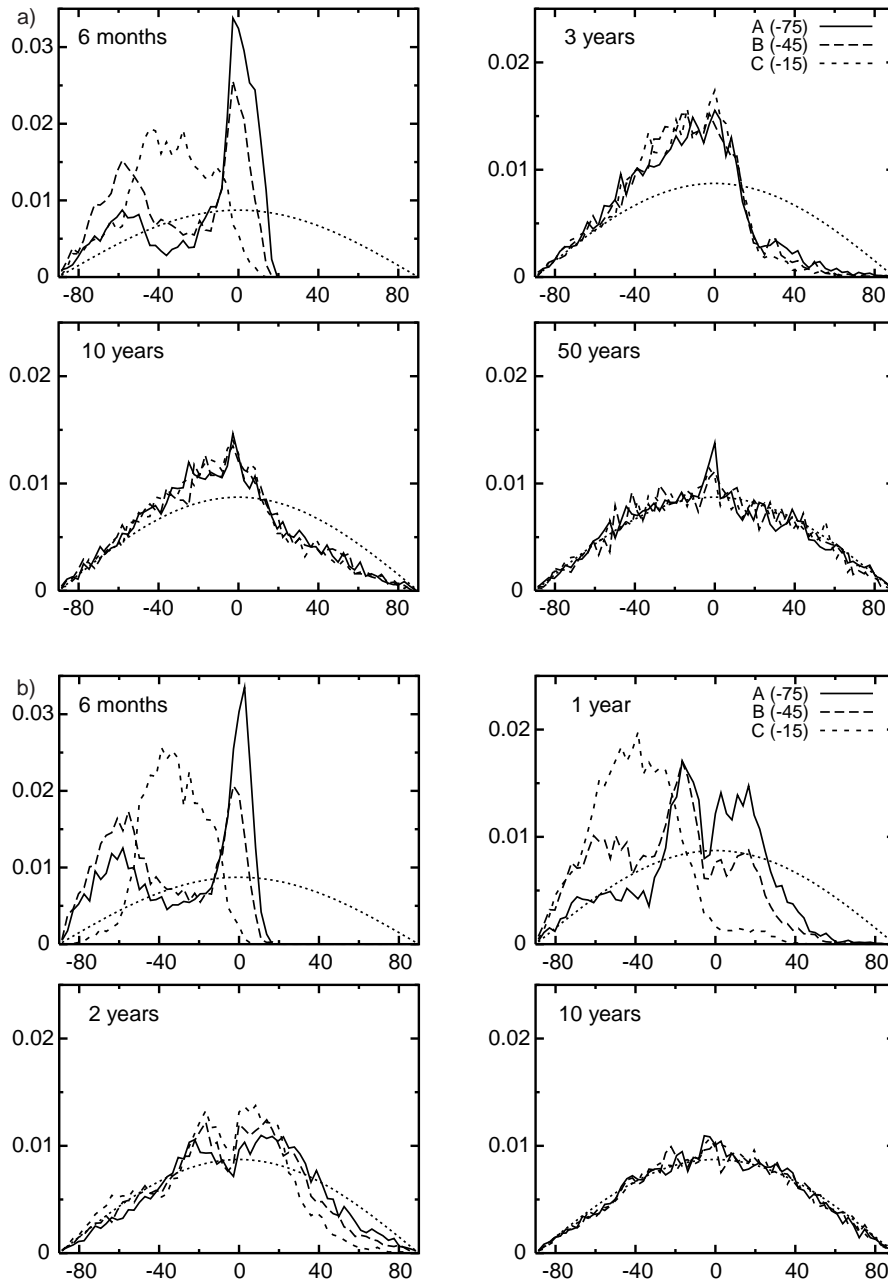


Fig. 3. – Latitudinal particle distribution at different times after release. The time is indicated in the figures. The three curves in each panel refer to three seeding latitudes (the solid line is for particles released at 75°S , the long-dashed line for particles released at 45°S , and the short-dashed line for particles released at 15°S). The dotted line is the distribution of a globally homogeneous tracer. Panels (a) are for perpetual forcing, panels (b) are for seasonally varying solar forcing.

and Hadley cell and reach the Equator, while others recirculate in the Ferrel cell and stay at mid-latitudes. In this sense, the edge between the Ferrel and Hadley cells constitutes a partial barrier to transport which may delay, at least on relatively short time scales and for the lower atmospheric levels, homogenization of particle distributions. Finally, particles released near the Equator (curve C in fig. 3) follow the upper branch of the Hadley cell and move, quite coherently, toward mid-latitudes, remaining at higher altitudes than those released at temperate and polar latitudes.

At later times, differences emerge between particle dynamics in perpetually forced and seasonal runs. For perpetual runs, the particle distribution first becomes homogeneous in the hemisphere where the particles have been released, with a very limited spread in the other hemisphere. Three years after release (second panel of fig. 3a), the three distributions of particles initially released at different latitudes have evolved toward a similar shape, indicating that homogenization has been achieved inside the hemisphere of origin. At later times, particles quietly spread into the other hemisphere. Fifty years after release (fourth panel of fig. 3a) the particle distribution has reached global homogeneity. This indicates that the Equator is a strong transport barrier in the perpetually forced situation.

By contrast, the behaviour of particle dynamics in the seasonal run does not display a clear stage of intra-hemispheric homogenization, as particles start to spread in the other hemisphere well before they homogenize in the hemisphere of origin (second panel of fig. 3b). One year after release, the particles originally seeded at mid and polar latitudes have started recirculating on both sides of the Equator, while particles originally seeded near the Equator are still mainly moving in the Southern hemisphere. Two years after release, the particle distribution has become almost homogeneous. This indicates that the Equator is a much weaker transport barrier for the (more realistic) seasonally varying solar forcing.

The difference between particle transport in perpetual and seasonally forced runs is made quantitative by plots of the time evolution of the r.m.s. difference between the particle distribution and the distribution of a globally fully-mixed passive tracer. Figures 4a), b) show the r.m.s. difference *vs.* time for latitudinal and vertical mixing in the case of perpetual forcing. Figures 4c), d) show the same quantities for seasonal forcing. The vertical distributions reach homogenization approximately at the same time, as seen from panels 4b), d). This is a signature of comparable intrahemispheric homogenization times for the two different forcings. While for perpetual forcing the latitudinal r.m.s. difference decreases very slowly, for the seasonal forcing the r.m.s. difference decreases to its final value after about two or three years, as already suggested by fig. 3b). This confirms the faster homogenization of seasonally forced runs and indicates that runs with perpetual forcing have an unrealistically large global homogenization time.

Another quantitative measure of the interhemispheric homogenization time is provided by the time evolution of the percentage of particles that are found in the opposite hemisphere with respect to where they have been released, the equilibrium value corresponding to full homogenization being 1/2. Figure 5a) shows the time evolution of the number of particles which are found in one hemisphere, having been initially seeded in the opposite one, divided by the total number of particles in that hemisphere at that time, for perpetual forcing. The value 1/2 is reached quite slowly, close to the end of the simulation time. Thus a typical global homogenization time for this type of forcing is of the order of 40 years.

Figure 5b) shows the percentage of particles found in the northern hemisphere for

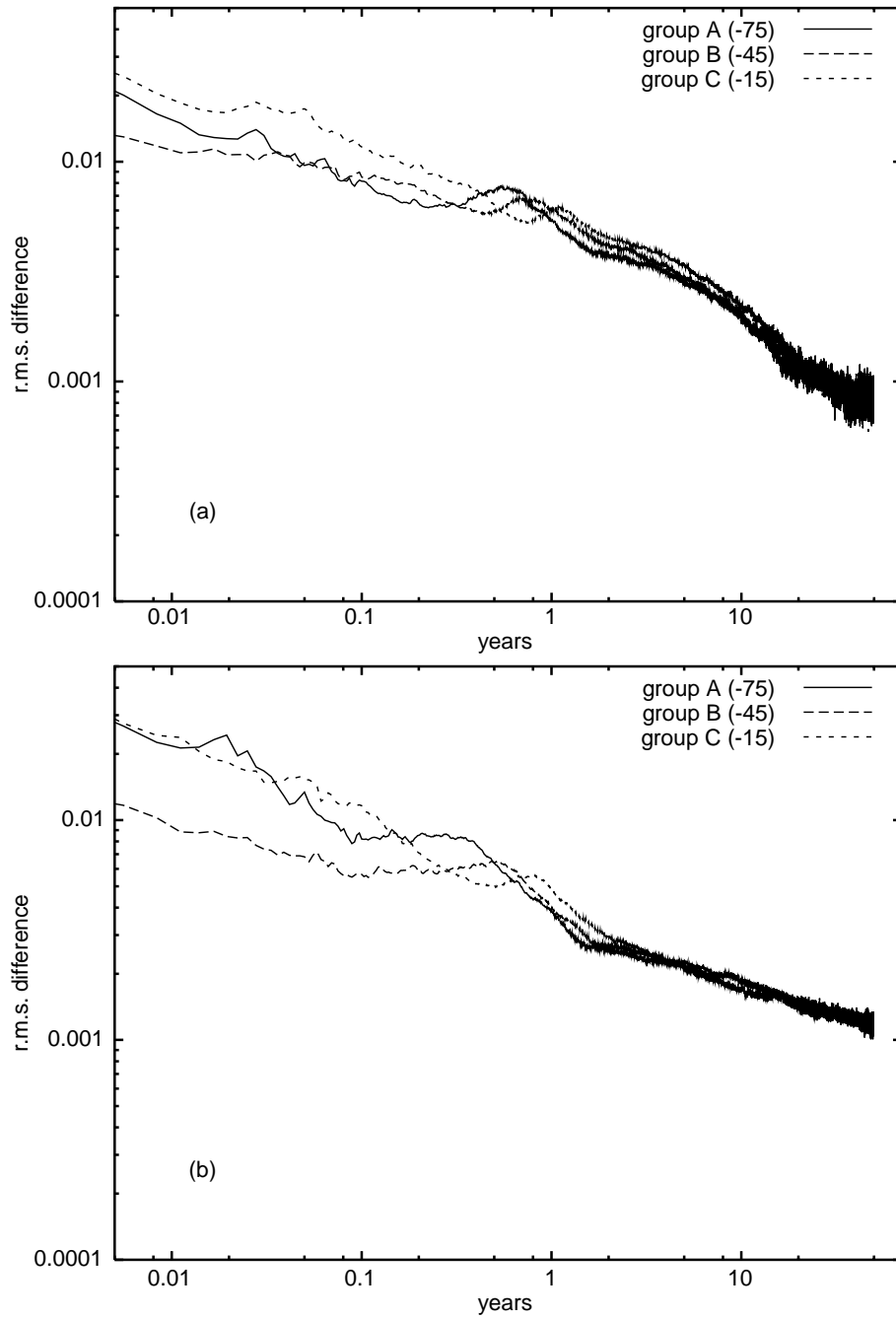


Fig. 4. – Time evolution of the r.m.s. difference between the particle distributions of fig. 3 and the distribution of a globally fully-mixed passive tracer. Panels (a, b) show the r.m.s. difference for latitudinal and vertical mixing in the case of perpetual forcing.

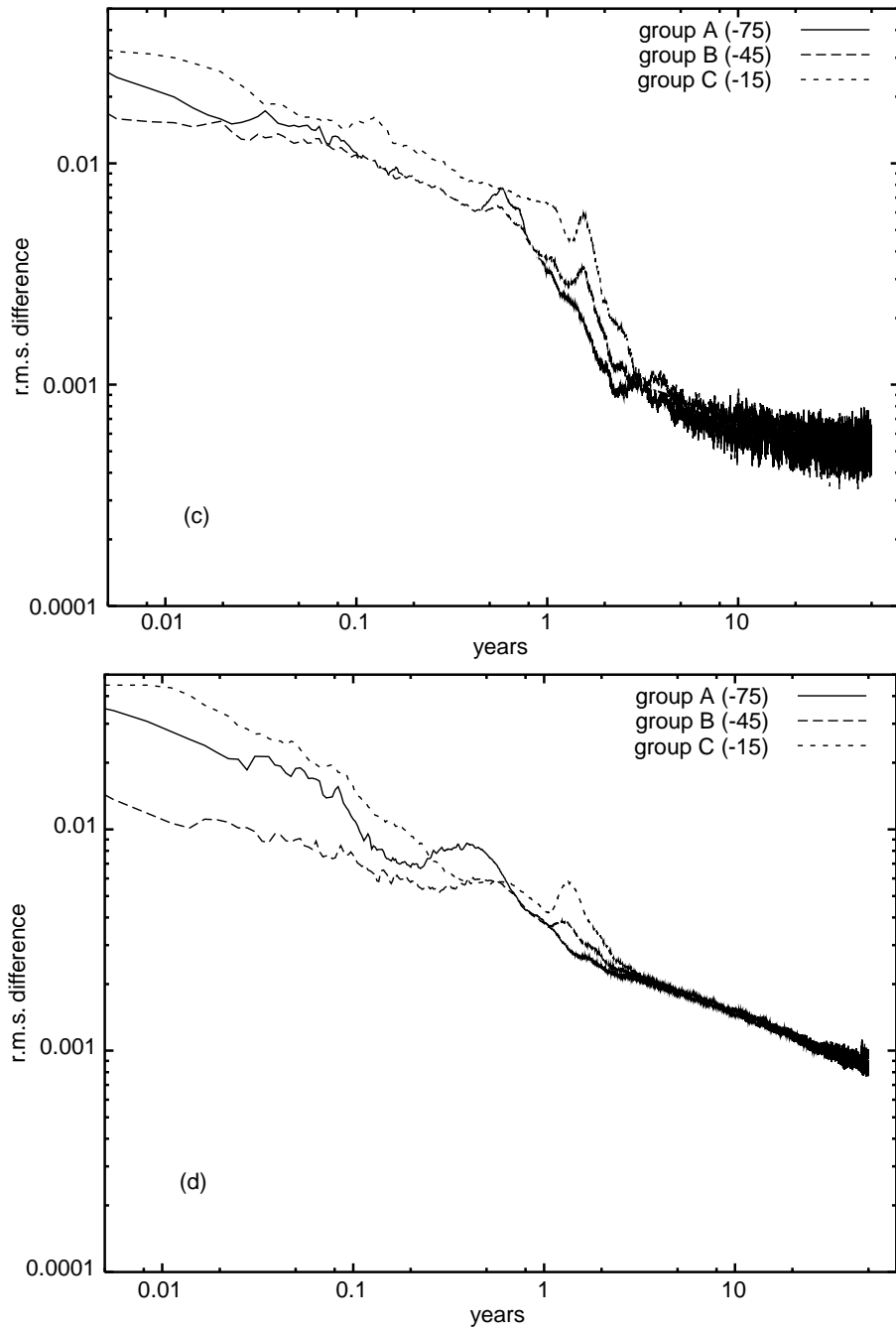


Fig. 4. – (Continued) Time evolution of the r.m.s. difference between the particle distributions of fig. 3 and the distribution of a globally fully-mixed passive tracer. Panels (c, d) show the same quantities for seasonal forcing.

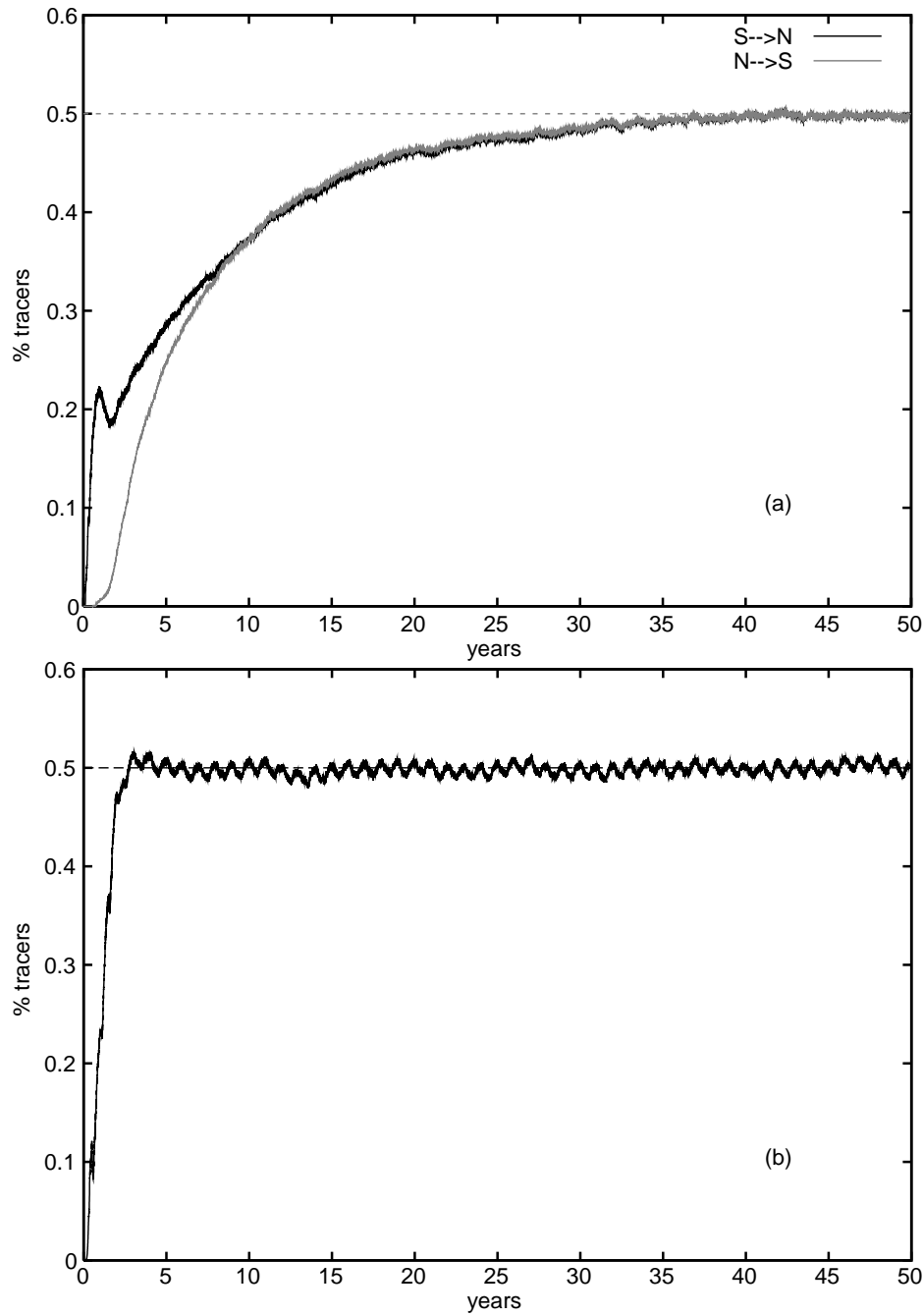


Fig. 5. – (a) Time evolution of the number of particles found in the hemisphere opposite to the one where particles have been seeded, divided by the total number of particles in that hemisphere at that time, for perpetual forcing. (b) Percentage of particles found in the northern hemisphere for the seasonally forced run.

the seasonally forced run (recall that in this case particles are released only in the southern hemisphere). In this case, homogenization is obtained after about two to three years. The small oscillation of tracer percentage between 48% and 52% is related to the annual oscillation of the climatological equator, due to the seasonal forcing. Superposed to this oscillation there is a faint evidence of a smaller variation over a longer timescale. This feature is reminiscent of the ultra-low-frequency variability detected in PUMA in ref. [16, 17].

5. – Properties of particle dispersion

Single-particle (absolute) meridional dispersion is defined as

$$(2) \quad A^2(t; t_0) = \langle [y_i(t + t_0) - y_i(t_0)]^2 \rangle,$$

where $y_i(t)$ is the meridional position of particle i at time t , t_0 is the release time, and the symbol $\langle . \rangle$ indicates average over the particle ensemble. Absolute dispersion provides information on the average distance that particles have traveled from their initial position. In isotropic, homogeneous and unbounded turbulence, the Taylor theorem [18] states that at short times dispersion is ballistic, $A^2 \propto t^2$ for $t \rightarrow 0$, and that at times larger than the Lagrangian decorrelation time dispersion becomes Brownian, $A^2 \propto t$ for $t \rightarrow \infty$. In bounded domains, absolute dispersion saturates at large times, $A^2(t) \rightarrow \text{const}$.

In the following, we are interested in the short-time properties of particle dispersion. Figure 6a) shows the meridional single-particle dispersion for the seasonally forced case. In each run, three ensembles of 30000 particles have been seeded at the three reference latitudes of 15°S, 45°S and 75°S. Particles have been released fifteen days after the beginning of southern hemisphere winter (first panel) and summer (second panel). The two straight lines in each panel indicate the ballistic and Brownian regimes. Figure 6b) shows a section of the potential vorticity (PV, solid lines) and isentropic (dashed lines) surfaces at the beginning of the two dispersion periods, respectively in winter and summer. The heavy solid points indicate the particle seeding sites.

We first discuss the winter situation. Particles released at 75°S start dispersing downward and equatorward along the isentrope passing through the seeding site. Here isentropes and PV isosurfaces are almost parallel and the dispersion is ballistic up to about three days. After this time, the dispersion is significantly slowed down, due to the fact that the particles meet the strong PV gradient at about 60°S, associated with the winter mid-latitude jet. The jet, however, has a lot of energetic mesoscale disturbances and in about eight days particles start spreading again, up to a time of about 20 days. Between about 20 and 100 days, particle dispersion is approximately arrested. Particles released at 45°S, by contrast, are in a region of strong PV gradient since the beginning. Thus, their dispersion has a smaller magnitude and it is approximately Brownian even at short times. Also for these particles, dispersion is arrested between about 20 and 100 days. During this period, the r.m.s. of the particle distribution (*i.e.*, the square root of absolute dispersion A^2) is about 20°. This behaviour can be associated with the fact that the particles have filled the Ferrel cell, and must now cross the barrier represented by the border between the Ferrel and the Hadley cells. In about three months, the particles cross this barrier and start spreading toward the Equator. At this point, dispersion grows again. Finally, particles released near the

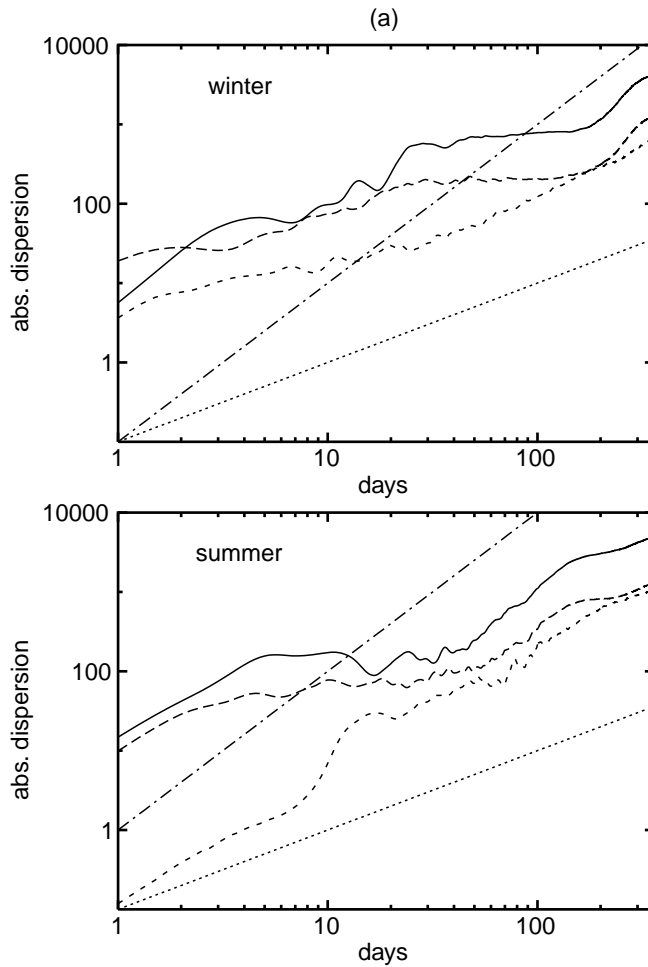


Fig. 6. – (a) Meridional single-particle dispersion for the seasonally forced case, for winter and summer initial conditions.

Equator have a smaller meridional dispersion due to the prevalence of vertical motions. They slowly spread southward at an approximately Brownian rate, remaining at higher tropospheric levels.

During summer, particles released at 75° and 45° S undergo approximately ballistic dispersion for a few days. Between about 4 and 40 days, these particles disperse very little. During summer, the PV gradient on isentropic surfaces is approximately homogeneous (see the second panel of fig. 6b), presumably being the main responsible of the slow dispersion on intermediate time scales. After about 40 days, the particles start dispersing again, filling their hemisphere of origin and starting spreading in the other hemisphere. At late times, dispersion becomes approximately Brownian. Analogously to what has been observed for winter conditions, particles released at 15° S disperse less than the others, undergoing Brownian diffusion already at early times.

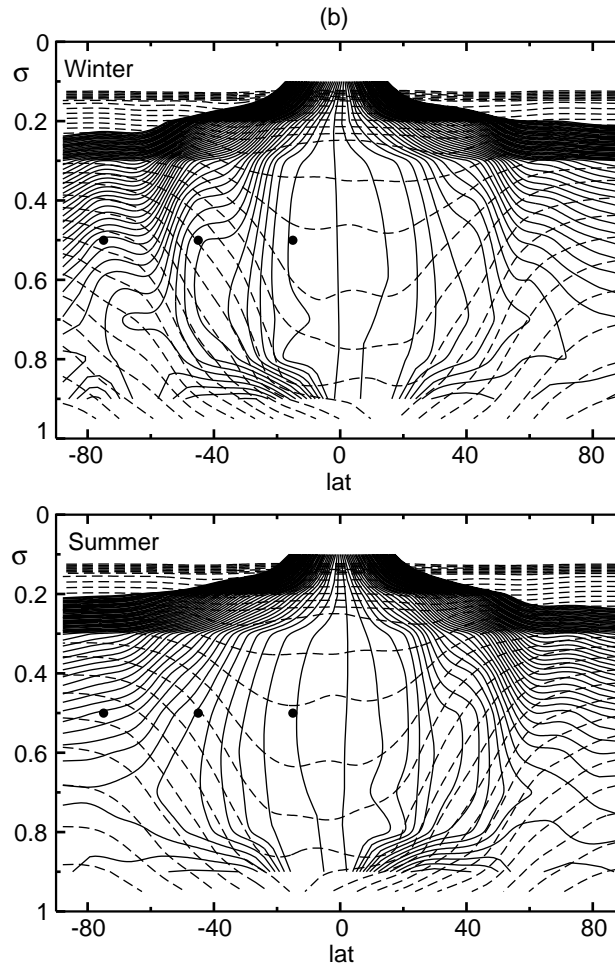


Fig. 6. – (Continued) (b) Section of the potential vorticity (solid lines) and isentropic (dashed lines) surfaces at the beginning of the two dispersion periods. The heavy solid points indicate the particle seeding sites.

At much larger times (not shown here), particle dispersion maintains a Brownian growth until homogenization is reached and the particles fill the surface of the sphere; at this point, dispersion is approximately arrested. A similar behaviour is observed for diffusion along σ levels.

6. – Conclusions

In this work we have studied the properties of tracer transport and homogenization in a simplified general circulation model of the atmosphere. We have shown that the particle dynamics is affected by the presence of several transport barriers, namely, the tropopause, the dynamical Equator, the edge between the Ferrel and the Hadley cell, and the winter mid-latitude jet. These barriers have different strength, and affect the particle motion on different time scales, leaving distinct signatures on particle dispersion.

An important difference has emerged between perpetual solar input and seasonally varying solar forcing. In the former case, the Equator is a particularly strong transport barrier, which delays global homogenization of passive tracers. For perpetual forcing, a typical global homogenization time is of the order of 40 years. By contrast, with seasonally varying forcing the Equator is more permeable, and homogenization is reached in about two to three years. In this latter case, the tracer does not homogenize inside one hemisphere before starting the global homogenization process. These results clearly indicate the need for using a seasonally varying solar forcing when studying long-term climatologies involving particle mixing.

REFERENCES

- [1] KNOBLOCH E. and WEISS J. B., *Transport by modulated traveling waves*, *Phys. Rev. A*, **36** (1987) 1522.
- [2] PIERREHUMBERT R. T., *Chaotic mixing of tracer and vorticity by modulated travelling Rossby waves*, *Geophys. Astrophys. Fluid Dyn.*, **58** (1991) 285.
- [3] PROVENZALE A., *Transport by coherent barotropic vortices*, *Ann. Rev. Fluid Mech.*, **31** (1999) 55.
- [4] WEISS J. B., *Hamiltonian maps and transport in structured fluids*, *Physica D*, **76** (1994) 230.
- [5] HOSKINS B. and SIMMONS A., *A multi-layer spectral model and the semi-implicit method*, *Q. J. Roy. Meteor. Soc.*, **101** (1975) 637.
- [6] JAMES I. N. and GRAY L., *Concerning the effect of surface drag in the circulation of a planetary atmosphere*, *Q. J. Roy. Meteor. Soc.*, **112** (1986) 1231.
- [7] FRISIUS T., LUNKEIT F., FRAEDRICH K. and JAMES I. N., *Storm-track organization and variability in a simplified atmospheric global circulation model*, *Q. J. Roy. Meteor. Soc.*, **124** (1998) 1019.
- [8] FRAEDRICH K., KIRK E. and LUNKEIT F., *PUMA: Portable University Model of the Atmosphere*, Deutsches Klimarechenzentrum, Technical Report, **16** (1998).
- [9] JAMES I. N. and DODD J. P., *A simplified global circulation model - User's Manual*, Dept. of Meteorology, University of Reading informal note (1993) 42 pp.
- [10] ELIASSEN E., MACHENAUER B. and RASMUSSEN E., *On a numerical method for integration of the hydrodynamical equations with a spectral representation of the horizontal fields*, *Inst. Th. Met. Univ. Copenhagen*, **101** (1970).
- [11] ORSZAG S. A., *Transform method for calculation of vector coupled sums: application to the spectral form of the vorticity equation*, *J. Atmos. Sci.*, **27** (1970) 890.
- [12] ROBERT A. J., ANDERSON J. and TURNBULL C., *An implicit time integration scheme for baroclinic modes of the atmosphere*, *Mon. Weath. Rev.*, **100** (1972) 329.
- [13] PEIXOTO J. P. and OORT A. H., *Physics of Climate* (American Institute of Physics, New York) 1992, 520 pp.
- [14] PIERREHUMBERT R. T. and YANG H., *Global Chaotic Mixing on Isoentropic Surfaces*, *J. Atmos. Sci.*, **50** (1991) 2462.
- [15] BOWMAN K. P. and COHEN P. J., *Interhemispheric exchange by seasonal modulation of the Hadley circulation*, *J. Atmos. Sci.*, **54** (1997) 2045.
- [16] JAMES P. M., FRAEDRICH K. and JAMES I. N., *Wave-zonal flow interaction and ultra-low frequency variability in a simplified global circulation model*, *Q. J. Roy. Meteor. Soc.*, **120** (1994) 1045.
- [17] JAMES P. M. and JAMES I. N., *Spatial structure of ultra-low frequency variability of the flow in a simple atmospheric circulation model*, *Q. J. Roy. Meteor. Soc.*, **118** (1992) 1211.
- [18] MONIN A. S. and YAGLOM A. M., *Statistical Fluid Mechanics* (MIT Press, Cambridge, MA) 1971, 769 pp.